OFDM-Based Generalized Optical MIMO

Chen Chen, *Member, IEEE*, Xin Zhong, Shu Fu, Xin Jian, Min Liu, Helin Yang, *Member, IEEE*, Arokiaswami Alphones, *Senior Member, IEEE*, and H. Y. Fu, *Senior Member, IEEE*

***Abstract*—The combination of multiple-input multiple-output (MIMO) transmission and orthogonal frequency division multiplexing (OFDM) modulation has been shown to be an effective way to substantially enhance the capacity of bandlimited optical wireless communication (OWC) systems. In this paper, we propose four OFDM-based generalized optical MIMO (GO-MIMO) techniques for intensity-modulation and direct-detection OWC systems, including OFDM-based frequency-domain generalized spatial modulation (FD-GSM), frequency-domain generalized spatial multiplexing (FD-GSMP), time-domain generalized spatial modulation (TD-GSM) and time-domain generalized spatial multiplexing (TD-GSMP). For OFDM-based FD-GSM and FD-GSMP, spatial mapping is performed in the frequency domain, while it is carried out in the time domain for OFDM-based TD-GSM and TD-GSMP. To efficiently estimate both spatial and constellation symbols in each OFDM-based GO-MIMO technique, a corresponding maximum-likelihood (ML) detection algorithm is designed. Extensive simulations are conducted to evaluate and compare the performance of OFDM-based GO-MIMO techniques under various MIMO settings in a typical indoor environment. Simulation results demonstrate that there exists an optimal GO-MIMO technique to achieve a target spectral efficiency for a given receiver location, and the obtained optimal GO-MIMO technique is also related to the specific location of the receiver.**

***Index Terms*—Optical wireless communication, orthogonal frequency division multiplexing, multiple-input multiple-output.**

I. Introduction

In recent years, we have witnessed an explosive growth of smart mobile devices in our daily life, which can provide many exciting services such as high definition video streaming, low-latency gaming, virtual/augmented reality (VR/AR) and Internet-of-things (IoT). In order to meet the demand for these data-greedy services, the requirement of mobile data traffic will face an exponential increase in the near future. It was predicted that the existing radio frequency (RF) spectrum will be saturated soon and the higher frequency part of the electromagnetic spectrum, i.e., the optical spectrum including visible light (VL), infrared (IR) and ultra-violet (UV), has revealed great potential to support the ever-increasing mobile data traffic [1]. Owing to its inherent capability to meet the demand of heavy data traffic, optical wireless communication (OWC) has been triggering tremendous interest in both academia and industry [2]. In typical OWC systems, light-emitting diodes (LEDs) or laser diodes (LDs) are usually used as transmitters and photo-diodes (PDs) are employed as receivers. More specifically, intensity modulation with direct detection (IM/DD) is generally adopted for signal transmission in OWC systems, and hence only real-valued and non-negative signals can be successfully transmitted [3]. Nevertheless, the achievable modulation bandwidth of commercial off-the-shelf (COTS) optical elements is relatively small, especially for white LEDs which usually have a 3-dB bandwidth of about several MHz [4]. In order to enhance the capacity of OWC systems with a relatively limited modulation bandwidth, the system spectral efficiency should be substantially enhanced.

So far, various techniques have been introduced in bandlimited IM/DD OWC systems for spectral efficiency enhancement, among which multiple-input multiple-output (MIMO) transmission and orthogonal frequency division multiplexing (OFDM) modulation are the two most popular ones. For MIMO transmission, several schemes have been widely considered, including repetition coding (RC), spatial modulation (SM) and spatial multiplexing (SMP) [5], [6]. Among them, RC is the simplest MIMO scheme, which can obtain transmit diversity. SM can be considered as a digitized MIMO scheme, where only a single transmitter is selected to transmit signal at each time instant, while SMP can achieve high multiplexing gain since different transmitters transmit different signals. For OFDM modulation, high-order quadrature amplitude modulation (QAM) constellations can be applied so as to improve the achievable spectral efficiency [7], [8]. Moreover, the combination of MIMO transmission and OFDM modulation has been further shown as an effective way to substantially enhance the spectral efficiency of bandlimited IM/DD OWC systems. For example, the combination of SM and OFDM was reported in [9]–[12], where the spatial mapping can be performed in the frequency domain, i.e., frequency-domain SM (FD-SM), or the time domain, i.e., time-domain SM (TD-SM). In [13]–[15], the combination of SMP and OFDM was also investigated, where different OFDM signals were transmitted in different SMP channels. In addition,

Manuscript received May 19, 2021; accepted July 5, 2021. Date of publication July 7, 2021; date of current version October 4, 2021. This work was supported in part by the National Natural Science Foundation of China under Grants 61901065 and 61701054, in part by the Fundamental Research Funds for the Central Universities under Grants 2021CDJQY-013, 2020CDJQY-A001 and 2020CDJGFWDZ014, and in part by Project funded by China Postdoctoral Science Foundation under Grant 2021M693744. *(Corresponding author: Chen Chen.)*

Chen Chen, Xin Zhong, Shu Fu, Xin Jian, and Min Liu are with the School of Microelectronics and Communication Engineering, Chongqing University, Chongqing 400044, China (e-mail: c.chen@cqu.edu.cn; 201912131098@cqu.edu.cn; shufu@cqu.edu.cn; jianxin@cqu.edu.cn; liumin@cqu.edu.cn).

Helin Yang and Arokiaswami Alphones are with the School of Electrical and Electronic Engineering, Nanyang Technological University, Singapore 639798, Singapore (e-mail: HYANG013@e.ntu.edu.sg; ealphones@ntu.edu.sg).

H. Y. Fu is with the Tsinghua-Berkeley Shenzhen Institute (TBSI), Tsinghua University, Shenzhen 518055, China (e-mail: hyfu@sz.tsinghua.edu.cn).

Color versions of one or more figures in this article are available at https://doi.org/10.1109/JLT.2021.3095359.

Digital Object Identifier 10.1109/JLT.2021.3095359

some other schemes that combine spatial/index modulation with OFDM have also been reported. For example, a generalized LED index modulation optical OFDM (GLIM-OFDM) scheme was proposed by using 4×4 MIMO in [16], where four LEDs are employed to transmit a complex time-domain OFDM signal. Although GLIM-OFDM has the advantages of requiring no Hermitian symmetry and DC bias, it can only be applied in the 4×4 MIMO system, where only the constellation bits encoded in the complex time-domain OFDM signal can be transmitted while no additional spatial bits can be transmitted. Furthermore, a pulse amplitude modulation (PAM)-based multiple-input single-output (MISO) SM system was investigated in [17], where an adaptive power allocation algorithm was proposed to solve the mobility problem. Although the SM transmission was applied in the MISO system, no additional spatial bits can be transmitted. In brief, only simple MIMO schemes such as SM and SMP have been mostly considered in the literature, which might not be able to fully explore the potential of MIMO transmission for spectral efficiency enhancement of bandlimited OWC systems.

Lately, the concept of generalized spatial modulation (GSM) has been proposed to enhance the performance of conventional SM [18]–[20], which has also been applied in OWC systems [21]–[23]. However, the definition of GSM in the current literature is not accurate. Specifically, the activated transmitters are assumed to transmit the same signal in the GSM defined in [18], [19], [22], [23], and meanwhile different signals can be transmitted by the activated transmitters in the GSM defined in [20], [21]. In this work, in order to distinguish the difference of these two categories of GSM schemes, we re-define them as follows: for the one where the activated transmitters transmit the same signal, we define it as "GSM"; for the one where the activated transmitters transmit different signals, we define it as "GSMP". Considering the superiority of GSM and GSMP in comparison to conventional MIMO techniques such as SM and SMP, it is of great significance to combine them with OFDM for bandlimited IM/DD OWC systems.

In this paper, we for the first time propose four OFDM-based generalized optical MIMO (GO-MIMO) techniques for bandlimited IM/DD OWC systems, including OFDM-based FD-GSM, FD-GSMP, TD-GSM and TD-GSMP. The proposed OFDM-based GO-MIMO techniques can be considered as the combination of OFDM modulation with two generalized MIMO techniques, i.e., GSM and GSMP, to achieve substantially enhanced spectral efficiency. Specifically, spatial mapping in OFDM-based FD-GSM and FD-GSMP is performed in the frequency domain, while it is executed in the time domain for OFDM-based TD-GSM and TD-GSMP.

The main contributions of this work can be summarized as follows:

- As an efficient combination of OFDM modulation and generalized MIMO transmission, the proposed OFDM-based GO-MIMO techniques can benefit from the advantages of both OFDM modulation and generalized MIMO transmission, making which very suitable for bandlimited IM/DD OWC systems.
- Maximum-likelihood (ML) detection algorithms are designed to efficiently estimate both spatial and constellation symbols for the proposed OFDM-based GO-MIMO techniques. Moreover, for OFDM-based FD-GSM and TD-GSM, maximal-ratio combining (MRC) is applied to achieve transmit diversity.
- Extensive simulation results are presented to evaluate and compare the performance of the proposed OFDM-based GO-MIMO techniques under various MIMO settings in a typical indoor environment.

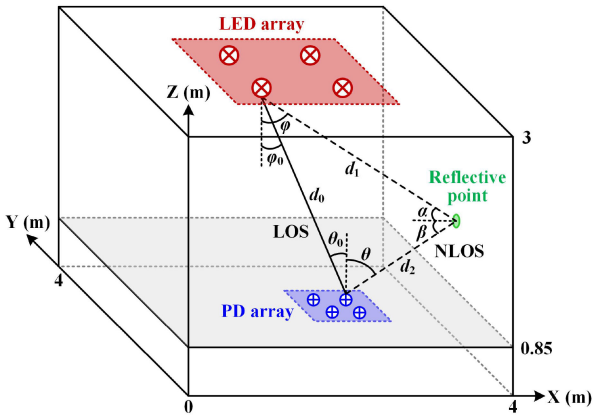

Fig. 1. Geometric setup of a general MIMO-OWC system.

The rest of this paper is organized as follows. In Section II, we describe the mathematical model of a general IM/DD-based MIMO-OWC system. In Section III, we propose four OFDM-based GO-MIMO techniques for OWC systems. Detailed simulation setup and results are presented in Section IV. Finally, Section V concludes the paper.

Notation: $(\cdot)^T$, $(\cdot)^*$ and $(\cdot)^\dagger$ represent the transpose, conjugated transpose and pseudo inverse of a vector or matrix, respectively. $(\cdot)^{-1}$ represents the inverse of a matrix. $\lfloor \cdot \rfloor$ and $\| \cdot \|_2$ denote the floor and modulus operators, respectively.

II. System Model

In this section, we describe the model of a general IM/DD-based MIMO-OWC system. Fig. 1 illustrates the geometric setup of a general MIMO-OWC system within a typical indoor environment, where the LED array consisting of N_t LEDs is mounted in the ceiling and the PD array consisting of N_r PDs is located over the receiving plane. Without loss of generality, we assume that the LEDs are point sources operating within their linear dynamic ranges and the overall system has a flat frequency response[1]. Moreover, we also assume that the LEDs are oriented vertically downwards while the PDs are oriented vertically upwards[2].

[1]The LED nonlinearity can be efficiently mitigated via pre-distortion [24] and a flat frequency response can be achieved by applying frequency-domain equalization techniques [25], [26].

[2]Random receiver orientation can have a significant impact on the performance of OWC (including MIMO-OWC) systems [27]. In this work, we mainly focus on the performance evaluation of OFDM-based GO-MIMO techniques. The impact of random receiver orientation on the performance of OFDM-based GO-MIMO techniques is beyond the scope of this work and it will be investigated in our future work.

Let $\mathbf{x} = [x_1, x_2, \ldots, x_{N_t}]^T$ be the transmitted signal vector, $\mathbf{H}$ represent the $N_r \times N_t$ MIMO channel matrix and $\mathbf{n} = [n_1, n_2, \ldots, n_{N_r}]^T$ denote the additive noise vector. The received signal vector $\mathbf{y} = [y_1, y_2, \ldots, y_{N_r}]^T$ can be obtained by

$$\mathbf{y} = \mathbf{H}\mathbf{x} + \mathbf{n}, \tag{1}$$

where the channel matrix of the $N_r \times N_t$ MIMO-OWC system can be expressed as follows:

$$\mathbf{H} = \begin{bmatrix} h_{11} & \cdots & h_{1N_t} \\ \vdots & \ddots & \vdots \\ h_{N_r1} & \cdots & h_{N_rN_t} \end{bmatrix}. \tag{2}$$

In (2), h_{rt} $(r = 1, 2, \ldots, N_r; t = 1, 2, \ldots, N_t)$ denotes the direct current (DC) channel gain between the r-th PD and the t-th LED. In a practical indoor environment, as shown in Fig. 1, h_{rt} generally consists of two components: one is the line-of-sight (LOS) component $h_{rt,\text{LOS}}$ and the other is the non-line-of-sight (NLOS) component $h_{rt,\text{NLOS}}$ [28]. Assuming that each LED follows the Lambertian radiation pattern, the LOS component $h_{rt,\text{LOS}}$ can be calculated by

$$h_{rt,\text{LOS}} = \begin{cases} \frac{(m+1)\rho A}{2\pi d_0^2}\cos^m(\varphi_0)T_s(\theta_0)g(\theta_0)\cos(\theta_0), \\ \text{for } 0 \le \theta_0 \le \Phi \\ 0, \quad \text{for } \theta_0 > \Phi \end{cases} \tag{3}$$

where $m = -\ln 2/\ln(\cos(\Psi))$ denotes the Lambertian emission order and Ψ is the semi-angle at half power of the LED; ρ and A are the responsivity and the active area of the PD, respectively; d_0 is the distance between the r-th PD and the t-th LED; φ_0 and θ_0 are the angle of irradiance and the incident angle, respectively; $T_s(\theta_0)$ is the gain of optical filter; $g(\theta_0) = \frac{n^2}{\sin^2\Phi}$ is the gain of optical lens, where n and Φ are the refractive index and the half-angle field-of-view (FOV) of the optical lens, respectively.

Moreover, the NLOS component $h_{rt,\text{NLOS}}$ can be obtained as follows [28]:

$$h_{rt,\text{NLOS}} = \begin{cases} \int \frac{(m+1)\rho\varepsilon A}{2(\pi d_1 d_2)^2}\cos^m(\varphi)\cos(\alpha)\cos(\beta)T_s(\theta)\times \\ g(\theta)\cos(\theta)dA_w, \quad \text{for } 0 \le \theta \le \Phi \\ 0, \qquad \text{for } \theta > \Phi \end{cases} \tag{4}$$

where d_1 is the distance between the reflective point and the t-th LED, d_2 is the distance between the r-th PD and the reflective point, ε is the reflectance coefficient of the wall, φ is the angle of irradiance from the LED, α is the incident angle to the reflective point, β is the angle of irradiance from the reflective point, and dA_w is a small reflective area on the wall [29].

To recover the transmitted signal vector $\mathbf{x}$, zero forcing (ZF) equalization is adopted at the receiver side for MIMO de-multiplexing [30], [31]. After applying ZF equalization, the estimate of $\mathbf{x}$ can be obtained as follows:

$$\hat{\mathbf{x}} = \mathbf{H}^{\dagger}\mathbf{y} = \mathbf{x} + \mathbf{H}^{\dagger}\mathbf{n}, \tag{5}$$

where $\mathbf{H}^{\dagger} = (\mathbf{H}^*\mathbf{H})^{-1}\mathbf{H}^*$ denotes the pseudo inverse of $\mathbf{H}$.

The additive noise in the IM/DD-based MIMO-OWC system usually consists of both shot and thermal noises, which can be reasonably modeled as a real-valued zero-mean additive white Gaussian noise (AWGN) with power $P_n = N_0 B$, where N_0 and B denote the noise power spectral density (PSD) and the modulation bandwidth, respectively.

TABLE I
FD-GSM MAPPING TABLE FOR $N_t = 4$ AND $N = 2$

Spatial bits	OFDM #1	OFDM #2	OFDM #3	OFDM #4
00	c	c	0	0
01	c	0	c	0
11	0	c	0	c
10	0	0	c	c

III. OFDM-BASED GO-MIMO TECHNIQUES

In this section, we introduce four OFDM-based GO-MIMO techniques, including OFDM-based FD-GSM, FD-GSMP, TD-GSM and TD-GSMP.

A. OFDM-Based FD-GSM

The first OFDM-based GO-MIMO technique is OFDM-based FD-GSM, where the GSM mapping is performed in the frequency domain, i.e., the subcarrier level. Fig. 2(a) illustrates the schematic diagram of the $N_r \times N_t$ OFDM-based FD-GSM system. For each subcarrier slot, the input bits are first separated and then mapped into a constellation symbol c and a spatial index vector $\mathbf{v}_F = [v_{1,F}, v_{2,F}, \ldots, v_{N,F}]^T$, where $v_{i,F} \in \{1, 2, \ldots, N_t\}$ and $v_{i,F} \neq v_{j,F}$ if $i \neq j$ for $i, j \in \{1, 2, \ldots, N\}$, with N denoting the number of selected OFDM modulators for constellation symbol transmission. Without loss of generality, we assume that the spatial indices in $\mathbf{v}_F$ are sorted in the ascending order, i.e., $v_{1,F} < v_{2,F} < \cdots < v_{N,F}$. After that, FD-GSM mapping is performed in the subcarrier level, where N out of totally N_t OFDM modulators are selected to transmit the same constellation symbol c while the inputs of the other OFDM modulators are set to zeros. Hence, letting $\mathbf{x}_F = [x_{1,F}, x_{2,F}, \ldots, x_{N_t,F}]^T$ denote the resultant transmit vector of N_t OFDM modulators for a given subcarrier slot, $x_{k,F}$ $(k = 1, 2, \ldots, N_t)$ can be obtained as follows:

$$x_{k,F} = \begin{cases} c, & \text{if } k = v_{i,F} \text{ for } i \in \{1, 2, \ldots, N\} \\ 0, & \text{otherwise} \end{cases}. \tag{6}$$

Table I shows the mapping table of FD-GSM for $N_t = 4$ and $N = 2$. As we can see, taking the spatial bits "01" as an example, the corresponding spatial index vector is given by $\mathbf{v}_F = [1, 3]^T$ and hence the OFDM modulators #1 and #3 are selected to transmit the same constellation symbol c while the inputs of the OFDM modulators #2 and #4 are set to zeros. As a result, the obtained transmit vector can be expressed by $\mathbf{x}_F = [c, 0, c, 0]^T$. After FD-GSM mapping, the N_t parallel data streams are modulated into digital OFDM signals, which are further converted to analog OFDM signals via digital-to-analog (D/A) conversion and subsequently utilized to drive N_t LED transmitters. It should be noted that OFDM-based FD-GSM with $N = 1$ becomes the conventional OFDM-based FD-SM as reported in [11].

Due to the IM/DD nature of typical MIMO-OWC systems, the Hermitian symmetry constraint is usually imposed at the input of inverse fast Fourier transform (IFFT) during OFDM modulation, in order to achieve IM/DD-compatible real-valued OFDM signals [7], [26], [32]. For the OFDM modulation with

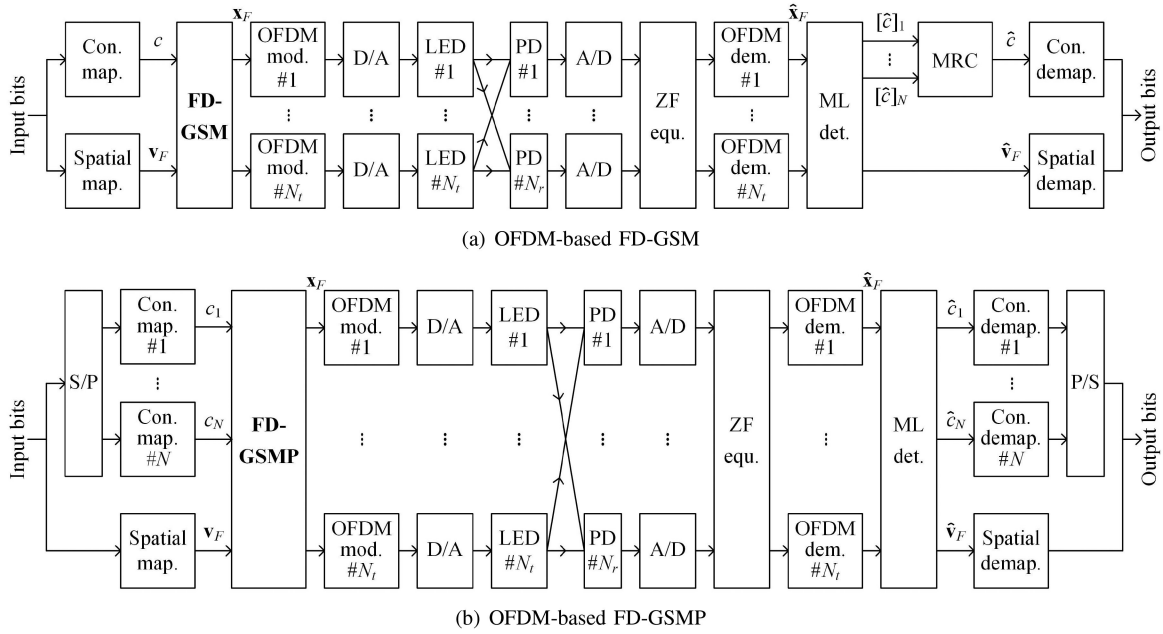

Fig. 2. Schematic diagrams of OFDM-based (a) FD-GSM and (b) FD-GSMP. Con.: constellation; map.: mapping; mod.: modulation; equ.: equalization; dem.: demodulation; det.: detection; demap.: demapping.

L-point IFFT, the input vector of IFFT can be expressed by

$$\mathbf{S} = [0, S_1, \ldots, S_{L/2-1}, 0, S^*_{L/2-1}, \ldots, S^*_1]^T. \tag{7}$$

It can be found that only $\frac{L}{2}-1$ subcarriers out of totally L subcarriers can be used for valid data transmission because of the imposed Hermitian symmetry constraint, and these subcarriers can be named as "data subcarriers". After performing IFFT, a real-valued bipolar time-domain signal can be generated as follows:

$$s_l = \frac{1}{\sqrt{L}} \sum_{k=0}^{L-1} S_k \exp\left(\frac{j2\pi kl}{L}\right), \tag{8}$$

where $l \in \{0, 1, \ldots, L-1\}$. When L is relatively large (e.g., $L > 64$), the time-domain signal follows a zero-mean Gaussian distribution with variance σ^2, i.e., $s_l \sim \mathcal{N}(0, \sigma^2)$. To convert the obtained bipolar OFDM signal into a unipolar one for intensity modulation in LED transmitters, a proper DC bias is generally introduced [33]. However, since OFDM signals exhibit relatively high peak-to-average power ratios (PAPRs), zero clipping is usually first executed to remove the excessive large negative samples in order to avoid the use of large DC biases. Hence, the biased and clipped time-domain sample can be given by

$$s'_l = \begin{cases} 0, & s_l < -b \\ s_l + b, & s_l \geq -b \end{cases}, \tag{9}$$

where $b = \alpha\sigma$ denotes the added DC bias with α being the proportionality constant. The DC bias in decibels is defined as $b_{\text{dB}} = 10\log_{10}(\alpha^2 + 1)$.

According to the spatial index vector $\mathbf{v}_F$, OFDM modulator selection is carried out in the subcarrier level. Since only $\frac{L}{2}-1$ subcarriers can be used for valid data transmission for a L-point IFFT in OFDM modulation, OFDM modulator selection can only be performed with respect to these $\frac{L}{2}-1$ subcarriers. As a result, the spectral efficiency (bits/s/Hz) of OFDM-based FD-GSM with N_t LEDs and M-ary constellation is given by

$$\begin{aligned} \eta_{\text{FD-GSM}} &= \frac{\frac{L}{2}-1}{L}\left(\log_2(M) + \lfloor \log_2(C(N_t, N)) \rfloor\right) \\ &\approx \underbrace{\frac{1}{2}\log_2(M)}_{\text{constellation}} + \underbrace{\frac{1}{2}\lfloor \log_2(C(N_t, N)) \rfloor}_{\text{spatial}}, \end{aligned} \tag{10}$$

where $\lfloor \cdot \rfloor$ denotes the floor operator which outputs an integer smaller or equal to its input value and $C(\cdot, \cdot)$ represents the binomial coefficient. The first term in (10) is contributed by the constellation symbols carried by $\frac{L}{2}-1$ subcarriers, while the second term is contributed by the spatial symbols. Moreover, the scaling factor $\frac{1}{2}$ corresponding to both the constellation and spatial symbols is due to the imposed Hermitian symmetry constraint in OFDM modulation [34].

At the receiver side, the radiated light is detected by N_r PDs and the resultant outputs are digitized via analog-to-digital (A/D) conversion. After ZF equalization and parallel OFDM demodulation, the estimate of the transmit vector $\mathbf{x}_F$ can be obtained by $\hat{\mathbf{x}}_F$, and ML detection is further performed to estimate the transmitted constellation symbol vector and spatial index vector. The detailed procedures to perform ML detection for OFDM-based FD-GSM are presented in Algorithm 1. The modulus vector $\mathbf{z}_F = [\|\hat{x}_{1,F}\|_2, \|\hat{x}_{2,F}\|_2, \ldots, \|\hat{x}_{N_t,F}\|_2]^T$ is first calculated, where $\|\cdot\|_2$ denotes the modulus operator, and then the elements of $\mathbf{z}_F$ are sorted in the descending order so as to obtain the sorted index vector $\mathbf{u} = [u_1, u_2, \ldots, u_{N_t}]^T$. Subsequently, the first N elements of $\mathbf{u}$ are abstracted and the corresponding index vector $\mathbf{u}' = [u_1, u_2, \ldots, u_N]^T$ can be obtained. We further sort the elements of $\mathbf{u}'$ in the ascending order and the sorted index vector yields the estimate of the transmitted spatial index vector, i.e., $\hat{\mathbf{v}}_F = [\hat{v}_1, \hat{v}_2, \ldots, \hat{v}_N]^T$.

Algorithm 1: ML detection for OFDM-based FD-GSM and FD-GSMP.

Input: $\hat{\mathbf{x}}_F = [\hat{x}_{1,F}, \hat{x}_{2,F}, \ldots, \hat{x}_{N_t,F}]^T$
Output: $[[\hat{c}]_1, [\hat{c}]_2, \ldots, [\hat{c}]_N]$, $[\hat{c}_1, \hat{c}_2, \ldots, \hat{c}_N]$, $\hat{\mathbf{v}}_F$
Calculate $\mathbf{z}_F = [\|\hat{x}_{1,F}\|_2, \|\hat{x}_{2,F}\|_2, \ldots, \|\hat{x}_{N_t,F}\|_2]^T$
Sort the elements of $\mathbf{z}_F$ in the descending order
Obtain the sorted index vector $\mathbf{u} = [u_1, u_2, \ldots, u_{N_t}]^T$
Abstract $\mathbf{u}' = [u_1, u_2, \ldots, u_N]^T$
Sort the elements of $\mathbf{u}'$ in the ascending order
Obtain the sorted index vector $\hat{\mathbf{v}}_F = [\hat{v}_1, \hat{v}_2, \ldots, \hat{v}_N]^T$ for both FD-GSM and FD-GSMP
for $i = 1$ to N **do**
  Obtain $[\hat{c}]_i = \hat{x}_{\hat{v}_i,F}$ for FD-GSM and $\hat{c}_i = \hat{x}_{\hat{v}_i,F}$ for FD-GSMP
end for

Moreover, the estimate of the transmitted constellation symbol vector, i.e., $[[\hat{c}]_1, [\hat{c}]_2, \ldots, [\hat{c}]_N]$, can be directly obtained by using $\hat{\mathbf{x}}_F$ and $\hat{\mathbf{v}}_F$. In order to achieve the final estimate of the transmitted constellation symbol c, i.e., $\hat{c}$, MRC is adopted to combine the N elements in $[[\hat{c}]_1, [\hat{c}]_2, \ldots, [\hat{c}]_N]$ [5], [35]. Finally, the output bits can be generated through constellation demapping and spatial demapping.

B. OFDM-Based FD-GSMP

In OFDM-based FD-GSM, multiple OFDM modulators can be selected to transmit the same constellation symbol and thus transmit diversity can be achieved in the frequency domain. Nevertheless, the achievable spectral efficiency contributed by constellation symbols is still the same as that of conventional SM, which limits the overall achievable spectral efficiency. In order to achieve enhanced overall spectral efficiency, the second OFDM-based GO-MIMO technique, i.e., OFDM-based FD-GSMP, is further proposed.

The schematic diagram of the $N_r \times N_t$ OFDM-based FD-GSMP system is shown in Fig. 2(b). As we can see, the input bits are first divided into two streams: one is for constellation mapping and the other is for spatial mapping. The serial bit stream for constellation mapping is further converted into N parallel bit streams via serial-to-parallel (S/P) conversion, which are then mapped into N parallel constellation symbols. Differing from OFDM-based FD-GSM where the N selected OFDM modulators are used to transmit the same constellation symbol, they are used to simultaneously transmit different constellation symbols in OFDM-based FD-GSMP. Letting $\mathbf{c} = [c_1, c_2, \ldots, c_N]^T$ denote the transmitted constellation symbol vector, for a given subcarrier slot, we can obtain the resultant transmit vector $\mathbf{x}_F = [x_{1,F}, x_{2,F}, \ldots, x_{N_t,F}]^T$ after FD-GSMP mapping as follows:

$$x_{k,F} = \begin{cases} c_i, & \text{if } k = v_{i,F} \text{ for } i \in \{1, 2, \ldots, N\} \\ 0, & \text{otherwise} \end{cases}, \tag{11}$$

for $k = 1, 2, \ldots, N_t$. The mapping table of FD-GSMP for $N_t = 4$ and $N = 2$ is given in Table II. Similarly, taking the spatial bits "01" as an example, the corresponding spatial index vector is still $\mathbf{v}_F = [1, 3]^T$, but the OFDM modulators #1 and #3 are selected to transit constellation symbols c_1 and c_2, respectively. Hence, the transmit vector is obtained by $\mathbf{x}_F = [c_1, 0, c_2, 0]^T$. Similarly, OFDM-based FD-GSMP also becomes OFDM-based FD-SM when $N = 1$ [11].

TABLE II
FD-GSMP MAPPING TABLE FOR $N_t = 4$ AND $N = 2$

Spatial bits	OFDM #1	OFDM #2	OFDM #3	OFDM #4
00	c_1	c_2	0	0
01	c_1	0	c_2	0
11	0	c_1	0	c_2
10	0	0	c_1	c_2

For FD-GSMP mapping, N out of N_t OFDM modulators are selected to transmit different constellation symbols and hence the spectral efficiency contributed by spatial symbols is the same for FD-GSM and FD-GSMP. However, since N different constellation symbols can be simultaneously transmitted for each subcarrier slot in FD-GSMP, the spectral efficiency contributed by constellation symbols for FD-GSMP becomes N times of that for FD-GSM. Therefore, the spectral efficiency (bits/s/Hz) of OFDM-based FD-GSMP with N_t LEDs and M-ary constellation is obtained by

$$\begin{aligned} \eta_{\text{FD-GSMP}} &= \frac{\frac{L}{2} - 1}{L} \left(N \log_2(M) + \lfloor \log_2(C(N_t, N)) \rfloor \right) \\ &\approx \underbrace{\frac{N}{2} \log_2(M)}_{\text{constellation}} + \underbrace{\frac{1}{2} \lfloor \log_2(C(N_t, N)) \rfloor}_{\text{spatial}}. \end{aligned} \tag{12}$$

After ZF equalization and parallel OFDM demodulation at the receiver side, ML detection is carried out to estimate the transmitted constellation symbol vector and spatial index vector for OFDM-based FD-GSMP. The detailed procedures of ML detection for OFDM-based FD-GSMP are the same as that of OFDM-based FD-GSM, which can be found in Algorithm 1. The N constellation symbols in the estimated constellation symbol vector $[\hat{c}_1, \hat{c}_2, \ldots, \hat{c}_N]$ are simultaneously demapped and the obtained parallel constellation bit streams are subsequently converted into a serial bit stream via parallel-to-serial (P/S) conversion. Moreover, the spatial bits can be directly obtained by demapping the estimated spatial index vector $\hat{\mathbf{v}}_F$.

C. OFDM-Based TD-GSM

In both OFDM-based FD-GSM and FD-GSMP, the spatial information is carried by OFDM modulator selection in the frequency domain[3] Due to the imposed Hermitian symmetry constraint, only approximately half of all the subcarriers can be utilized to carry valid data and hence OFDM modulator selection can only be performed with respect to these subcarriers. As a

[3]Note that the proposed OFDM-based FD-GSM/GSMP schemes are essentially different from the well-known OFDM with index modulation scheme [36], [37]. In OFDM with index modulation, the "index" refers to the index of the subcarriers and only a subset of the data subcarriers within each OFDM block can be used to transmit constellation symbols. However, in OFDM-based FD-GSM/GSMP, the "index" refers to the index of the OFDM modulators corresponding to the LED transmitters and all the data subcarriers within each OFDM block can be used to transmit constellation symbols.

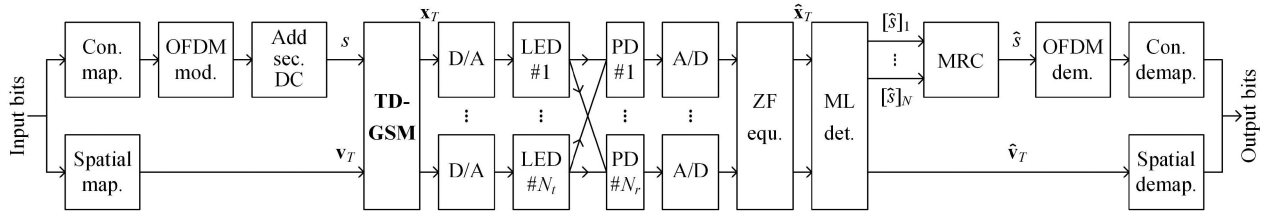

(a) OFDM-based TD-GSM

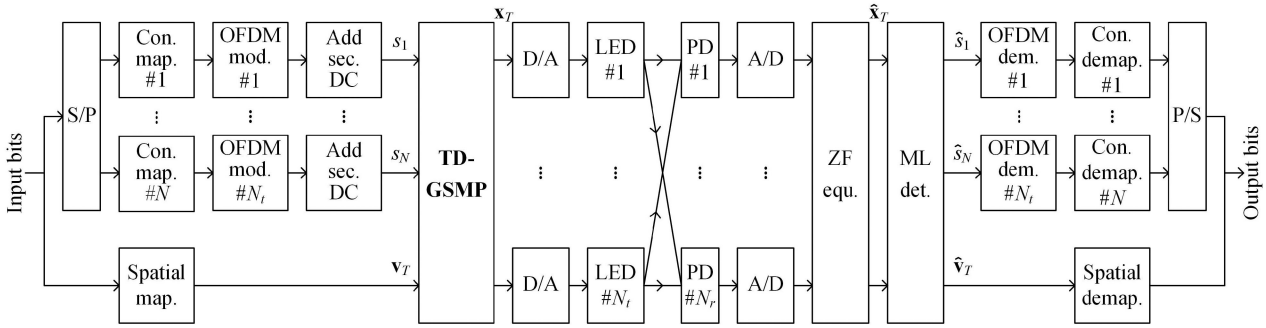

(b) OFDM-based TD-GSMP

Fig. 3. Schematic diagrams of OFDM-based (a) TD-GSM and (b) TD-GSMP. Con.: constellation; map.: mapping; mod.: modulation; sec.: secondary; equ.: equalization; dem.: demodulation; det.: detection; demap.: demapping.

result, the spectral efficiency contributed by spatial symbols in both OFDM-based FD-GSM and FD-GSMP is inevitably halved. To eliminate the impact of the imposed Hermitian symmetry constraint and hence achieve enhanced spectral efficiency contributed by spatial symbols, we propose the third OFDM-based GO-MIMO technique, i.e., OFDM-based TD-GSM.

Fig. 3(a) shows the schematic diagram of the $N_r \times N_t$ OFDM-based TD-GSM system, where the spatial information is encoded in the time domain via LED transmitter selection. More specifically, for each time slot, N out of totally N_t LED transmitters are selected to transmit the same time-domain sample while the other LEDs are not activated. To successfully encode the spatial information, the transmitted time-domain sample should be non-zero. It can be seen from (9) that the biased and clipped time-domain OFDM signal might have a few zero elements due to zero clipping. When the time-domain samples are zero or very small, the spatial information might be lost. Hence, a secondary DC bias can be added after OFDM modulation so as to guarantee that all the time-domain samples have positive values [11]. After adding a secondary DC bias, (9) can be modified as follows:

$$s_l' = \begin{cases} \epsilon, & x_l < -b \\ x_l + b + \epsilon, & x_l \geq -b \end{cases}, \tag{13}$$

where $\epsilon = \rho b$ is the value of the secondary DC bias with ρ denoting the ratio between the secondary DC bias (i.e., ϵ) and the primary DC bias (i.e., b).

Letting s and $\mathbf{v}_T = [v_{1,T}, v_{2,T}, \ldots, v_{N,T}]^T$ respectively denote the time-domain sample and the spatial index vector, for a given time slot, the resultant transmit vector of N_t LED transmitters $\mathbf{x}_T = [x_{1,T}, x_{2,T}, \ldots, x_{N_t,T}]^T$ after TD-GSM mapping can be obtained by

$$x_{k,T} = \begin{cases} s, & \text{if } k = v_{i,T} \text{ for } i \in \{1, 2, \ldots, N\} \\ 0, & \text{otherwise} \end{cases}, \tag{14}$$

TABLE III
TD-GSM MAPPING TABLE FOR $N_t = 4$ AND $N = 2$

Spatial bits	LED #1	LED #2	LED #3	LED #4
00	s	s	0	0
01	s	0	s	0
11	0	s	0	s
10	0	0	s	s

for $k = 1, 2, \ldots, N_t$. The corresponding mapping table of TD-GSM for $N_t = 4$ and $N = 2$ can be found in Table III. Taking the spatial bits "01" as an example, the spatial index vector is given by $\mathbf{v}_T = [1, 3]^T$ and hence the LED transmitters #1 and #3 are selected to transit the same time-domain sample s while the inputs of the LED transmitters #2 and #4 are set to zeros. Hence, the obtained transmit vector can be given by $\mathbf{x}_T = [s, 0, s, 0]^T$. Note that OFDM-based TD-GSM becomes OFDM-based TD-SM when $N = 1$ [11].

In OFDM-based TD-GSM, LED transmitter selection can be performed with respect to all the time-domain samples and hence the spectral efficiency contributed by spatial symbols is doubled in comparison to that of both OFDM-based FD-GSM and FD-GSMP. Therefore, the spectral efficiency (bits/s/Hz) of OFDM-based TD-GSM with N_t LEDs and M-ary constellation can be given by

$$\begin{aligned} \eta_{\text{TD-GSM}} &= \frac{\frac{L}{2} - 1}{L} \log_2(M) + \lfloor \log_2(C(N_t, N)) \rfloor \\ &\approx \underbrace{\frac{1}{2} \log_2(M)}_{\text{constellation}} + \underbrace{\lfloor \log_2(C(N_t, N)) \rfloor}_{\text{spatial}}. \end{aligned} \tag{15}$$

At the receiver side, ML detection is performed right after ZF equalization for OFDM-based TD-GSM and the detailed

Algorithm 2: ML detection for OFDM-based TD-GSM and TD-GSMP.

Input: $\hat{\mathbf{x}}_T = [\hat{x}_{1,T}, \hat{x}_{2,T}, \ldots, \hat{x}_{N_t,T}]^T$
Output: $[[\hat{s}]_1, [\hat{s}]_2, \ldots, [\hat{s}]_N]$, $[\hat{s}_1, \hat{s}_2, \ldots, \hat{s}_N]$, $\hat{\mathbf{v}}_T$
Sort the elements of $\hat{\mathbf{x}}_T$ in the descending order
Obtain the sorted index vector $\mathbf{w} = [w_1, w_2, \ldots, w_{N_t}]^T$
Abstract $\mathbf{w}' = [w_1, w_2, \ldots, w_N]^T$
Sort the elements of $\mathbf{w}'$ in the ascending order
Obtain the sorted index vector $\hat{\mathbf{v}}_T = [\hat{v}_1, \hat{v}_2, \ldots, \hat{v}_N]^T$ for both TD-GSM and TD-GSMP
for $i = 1$ to N **do**
  Obtain $[\hat{s}]_i = \hat{x}_{\hat{v}_i,T}$ for TD-GSM and $\hat{s}_i = \hat{x}_{\hat{v}_i,T}$ for TD-GSMP
end for

procedures are given in Algorithm 2. Considering that the transmitted time-domain samples have non-negative values, we can directly sort the elements of the estimated transmit vector $\hat{\mathbf{x}}_T = [\hat{x}_{1,T}, \hat{x}_{2,T}, \ldots, \hat{x}_{N_t,T}]^T$ in the descending order and obtain the corresponding sorted index vector $\mathbf{w} = [w_1, w_2, \ldots, w_{N_t}]^T$. The abstracted index vector $\mathbf{w}' = [w_1, w_2, \ldots, w_N]^T$ can be further achieved by abstracting the first N elements of $\mathbf{w}$, which is then sorted in the ascending order to yield the sorted index vector $\hat{\mathbf{v}}_T = [\hat{v}_1, \hat{v}_2, \ldots, \hat{v}_N]^T$. By employing $\hat{\mathbf{x}}_T$ and $\hat{\mathbf{v}}_T$, the estimate of the transmitted time-domain sample vector $[[\hat{s}]_1, [\hat{s}]_2, \ldots, [\hat{s}]_N]$ can be obtained. Given the N estimated time-domain samples, MRC is applied to generate the final estimate of the transmitted time-domain sample, i.e., $\hat{s}$.

D. OFDM-Based TD-GSMP

Similar to OFDM-based FD-GSM, OFDM-based TD-GSM can only achieve transmit diversity in the time domain while the overall achievable spectral efficiency is still limited. Hence, the fourth OFDM-based GO-MIMO technique, i.e., OFDM-based TD-GSMP, is finally proposed.

The schematic diagram of the $N_r \times N_t$ OFDM-based TD-GSMP system is depicted in Fig. 3(b), where the serial bit stream for constellation mapping is converted into N parallel bit streams via S/P conversion and each bit stream undergoes constellation mapping, OFDM modulation and secondary DC bias addition. In OFDM-based TD-GSMP, the N selected LED transmitters are used to simultaneously transmit different time-domain samples. Letting $\mathbf{s} = [s_1, s_2, \ldots, s_N]^T$ denote the transmitted time-domain sample vector, for a given time slot, the resultant transmit vector $\mathbf{x}_T = [x_{1,T}, x_{2,T}, \ldots, x_{N_t,T}]^T$ after TD-GSMP mapping can be obtained as follows:

$$x_{k,T} = \begin{cases} s_i, & \text{if } k = v_{i,F} \text{ for } i \in \{1, 2, \ldots, N\} \\ 0, & \text{otherwise} \end{cases}, \tag{16}$$

for $k = 1, 2, \ldots, N_t$. Table IV gives the mapping table of TD-GSMP for $N_t = 4$ and $N = 2$. For input spatial bits "01," the spatial index vector is $\mathbf{v}_T = [1, 3]^T$ and the LED transmitters #1 and #3 are selected to transit time-domain samples s_1 and s_2, respectively. As a result, the corresponding transmit vector is given by $\mathbf{x}_T = [s_1, 0, s_2, 0]^T$. Similarly, OFDM-based TD-GSMP also becomes OFDM-based TD-SM when $N = 1$ [11].

TABLE IV
TD-GSMP MAPPING TABLE FOR $N_t = 4$ AND $N = 2$

Spatial bits	LED #1	LED #2	LED #3	LED #4
00	s_1	s_2	0	0
01	s_1	0	s_2	0
11	0	s_1	0	s_2
10	0	0	s_1	s_2

For TD-GSMP mapping, N out of N_t LED transmitters are selected to transmit different time-domain samples for each time slot, and hence the spectral efficiency (bits/s/Hz) of OFDM-based TD-GSMP with N_t LEDs and M-ary constellation can be achieved by

$$\begin{aligned} \eta_{\text{TD-GSMP}} &= \frac{\frac{L}{2} - 1}{L} N \log_2(M) + \lfloor \log_2(C(N_t, N)) \rfloor \\ &\approx \underbrace{\frac{N}{2} \log_2(M)}_{\text{constellation}} + \underbrace{\lfloor \log_2(C(N_t, N)) \rfloor}_{\text{spatial}}. \end{aligned} \tag{17}$$

After ZF equalization at the receiver side, ML detection is performed to estimate the transmitted time-domain sample vector and spatial index vector for OFDM-based TD-GSMP. The detailed procedures of ML detection for OFDM-based TD-GSMP are the same as that of OFDM-based TD-GSM, which can be found in Algorithm 2. After OFDM demodulation, constellation demapping and P/S conversion, the serial constellation bit stream can be obtained. In addition, the spatial bits can be generated via spatial demapping.

IV. SIMULATION RESULTS

In this section, we evaluate and compare the performance of the proposed OFDM-based GO-MIMO techniques in a typical indoor MIMO-OWC system via numerical simulations. Moreover, the following relevant benchmark schemes have been adopted for performance comparison which can be viewed as the special cases of the proposed OFDM-based GO-MIMO techniques: 1) RC, which is the same as both FD-GSM and TD-GSM with $N = N_t$ [5]; 2) SMP, which is the same as both FD-GSMP and TD-GSMP with $N = N_t$ [5]; 3) FD-SM, which is the same as both FD-GSM and FD-GSMP with $N = 1$ [11], [12]; 4) TD-SM, which is the same as both TD-GSM and TD-GSMP with $N = 1$ [11], [12].

A. Simulation Setup

In our simulations, we setup the MIMO-OWC systems in a typical indoor room. The geometric setup can be found in Fig. 1, where the room has a dimension of 4 m × 4 m × 3 m and the receiving plane is 0.85 m above the floor. The LED array is mounted at the center of the ceiling and the user equipped with a PD array is located over the receiving plane. The key simulation parameters are listed in Table V.

In the following performance evaluations, two MIMO settings, i.e., 2×2 MIMO and 4×4 MIMO, are considered.

TABLE V
SIMULATION PARAMETERS

Parameter	Value
Room dimension	4 m × 4 m × 3 m
Height of receiving plane	0.85 m
Semi-angle at half power of LED	65°
LED spacing	2 m
Gain of optical filter	0.9
Refractive index of optical lens	1.5
Half-angle FOV of optical lens	65°
Responsivity of APD	15 A/W
Active area of APD	19.6 mm^2
APD spacing	10 cm
Reflectance coefficient of wall	0.8
Modulation bandwidth	20 MHz
Noise power spectral density	10^{-22} A^2/Hz

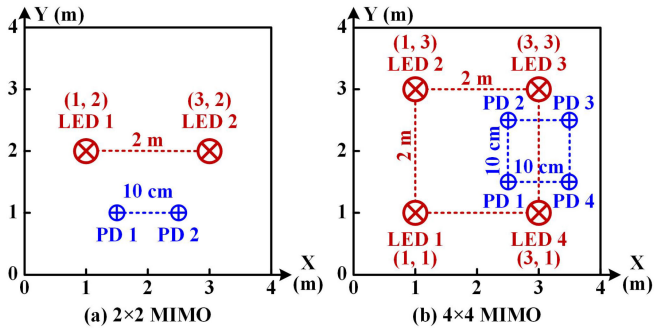

Fig. 4. Top view of (a) 2×2 MIMO and (b) 4×4 MIMO.

Figs. 4(a) and (b) depict the top views of the 2×2 and 4×4 MIMO settings, respectively. As we can see, for both the 2×2 and 4×4 MIMO settings, the spacing between two adjacent LEDs is 2 m and the spacing between two adjacent PDs is 10 cm. In order to achieve full coverage, both the semi-angle at half power of the LED and the half-angle FOV of the optical lens are set to 65°.

Due to the high channel correlation in typical MIMO-OWC systems, a large signal-to-noise ratio (SNR) is usually required to achieve a high spectral efficiency [5], [6]. In order to obtain a relatively large SNR at the receiver side, high-sensitivity avalanche PDs (APDs) are adopted in the system. Specifically, the APDs are assumed to have a responsivity of 15 A/W and an active area of 19.6 mm^2. Note that these two values are the practical parameters of a commercially available APD used in the experiments reported in [38].

Moreover, the gain of the optical filter and the refractive index of the optical lens are set to 0.9 and 1.5, respectively. The reflectance coefficient of the wall is assumed to be 0.8 [29]. The modulation bandwidth is set to 20 MHz[4] and the noise PSD is 10^{-22} A^2/Hz [5].

B. Spectral Efficiency

We first investigate the spectral efficiency of the proposed OFDM-based GO-MIMO techniques in the MIMO-OWC system with M-ary constellation under different MIMO settings.

[4]A 20-MHz modulation bandwidth can be achieved by using a commercially available white LED with frequency-domain pre-equalization, as experimentally reported in [26]

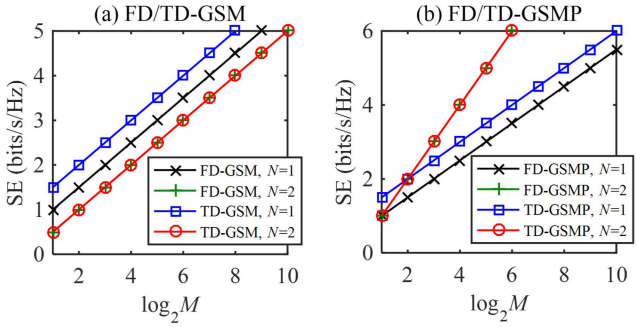

Fig. 5. Spectral efficiency (SE) vs. $\log_2 M$ for OFDM-based 2×2 MIMO with (a) FD-GSM and TD-GSM and (b) FD-GSMP and TD-GSMP.

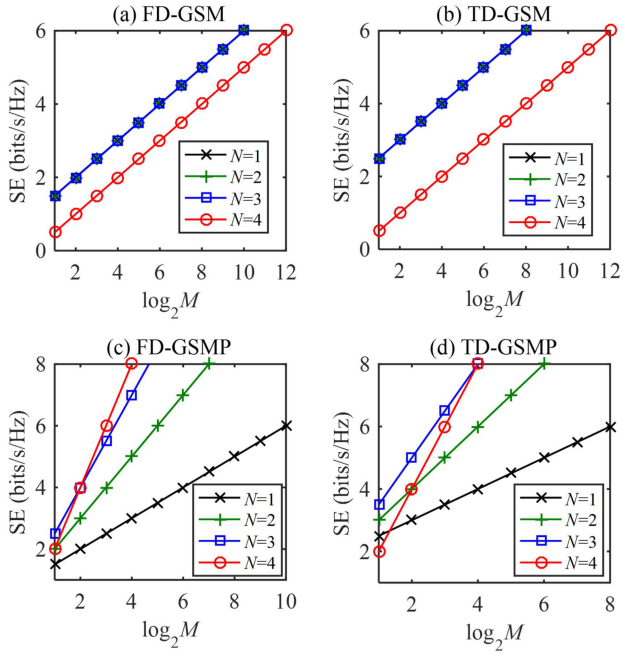

Fig. 6. Spectral efficiency (SE) vs. $\log_2 M$ for OFDM-based 4×4 MIMO with (a) FD-GSM, (b) TD-GSM, (c) FD-GSMP and (d) TD-GSMP.

Fig. 5 shows the spectral efficiency versus $\log_2 M$ for different OFDM-based GO-MIMO techniques under the 2×2 MIMO setting. It can be found that FD-GSM and TD-GSM achieve the same spectral efficiency with $N = 2$, while the spectral efficiency of TD-GSM is 0.5-bit/s/Hz higher than that of FD-GSM when $N = 1$ for a given M. Similarly, the spectral efficiencies of FD-GSMP and TD-GSMP are the same with $N = 2$, which greatly outperform the spectral efficiencies of both FD-GSMP and TD-GSMP with $N = 1$ for a relatively large M value. Fig. 6 shows the spectral efficiency versus $\log_2 M$ under the 4×4 MIMO setting. For FD-GSM, the spectral efficiencies are the same with $N = 1$, 2 and 3, which are 1-bit/s/Hz higher than that with $N = 4$ for a given M. It is the same for TD-GSM that the same spectral efficiencies are obtained with $N = 1$, 2 and 3, which are higher than that with $N = 4$ for a given M, and the only difference is that the spectral efficiency improvement becomes 2 bits/s/Hz. Moreover, different spectral efficiencies can be achieved with different N values for FD-GSMP and

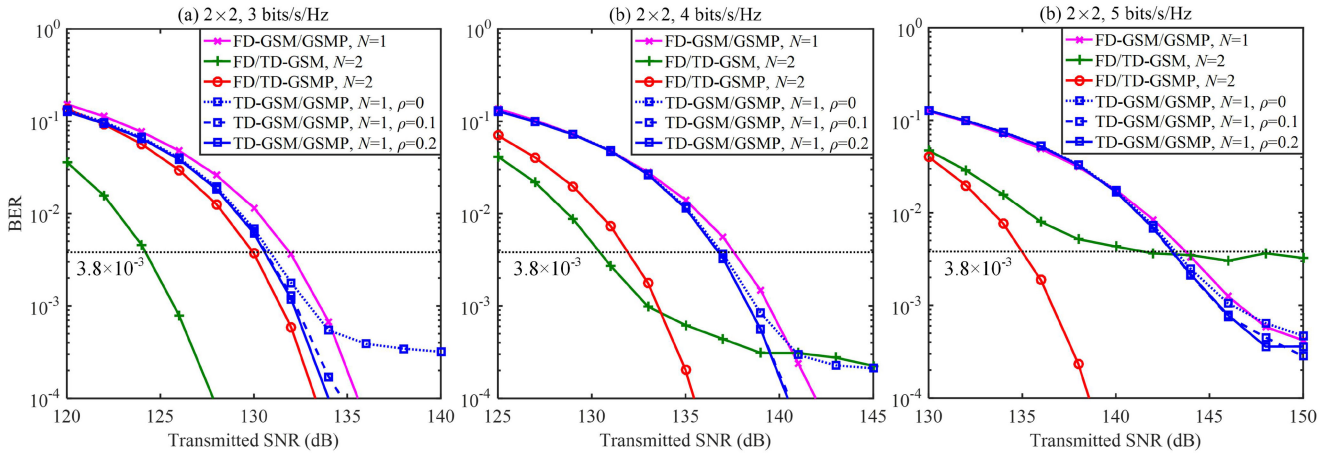

Fig. 7. BER vs. transmitted SNR for OFDM-based 2×2 GO-MIMO at the receiver location of (1.5 m, 1.5 m, 0.85 m) with a spectral efficiency of (a) 3 bits/s/Hz, (b) 4 bits/s/Hz, and (c) 5 bits/s/Hz.

TD-GSMP. For a given M, TD-GSMP generally achieves a higher spectral efficiency than FD-GSMP.

For the bit error rate (BER) performance evaluation in the following subsection, we consider different spectral efficiencies for each MIMO setting, and the corresponding required M values for each OFDM-based GO-MIMO technique can be directly obtained from Figs. 5 and 6.

C. BER Performance

Based on the above spectral efficiency analysis, we further investigate and compare the BER performance of the proposed OFDM-based GO-MIMO techniques in the MIMO-OWC systems described in Section IV-A. In typical indoor MIMO-OWC systems, the channel gain defined by (4) might be different for different LED/PD pairs due to the specific distance and emission/incident angle of each LED/PD pair. Hence, the received SNRs corresponding to different LED/PD pairs might be different. To ensure a fair performance comparison of different OFDM-based GO-MIMO techniques, we evaluate the BER performance with respect to the transmitted SNR [5]. Specifically, transmitted SNR is defined as the ratio of the transmitted electrical signal power P_s to the additive noise power P_n, i.e., P_s/P_n. Moreover, in order to achieve a trade-off between peak clipping and clipping distortion, a moderate primary DC bias of $b_{\text{dB}} = 10$ dB is adopted in the following evaluations [12]. In addition, the 7% forward error correction (FEC) coding limit of 3.8×10^{-3} is adopted as the BER threshold to compare the performance of different OFDM-based GO-MIMO techniques [39].

In the next, we evaluate the BER performance of OFDM-based GO-MIMO techniques under different MIMO settings. Fig. 7 shows the BER versus transmitted SNR for OFDM-based 2×2 GO-MIMO at the receiver location of (1.5 m, 1.5 m, 0.85 m) with different spectral efficiencies. For a spectral efficiency of 3 bits/s/Hz, FD/TD-GSM with $N = 2$ (i.e., RC) achieves the best BER performance, which outperforms FD/TD-GSMP with $N = 2$ (i.e., SMP) by an SNR gain of 5.8 dB at BER $= 3.8 \times 10^{-3}$. Moreover, TD-GSM/GSMP with $N = 1$ (i.e., TD-SM) outperforms FD-GSM/GSMP with $N = 1$ (i.e., FD-SM), and the performance of TD-GSM/GSMP with $N = 1$ can be slightly improved when ρ is increased from 0 to 0.1. However, further increasing ρ to 0.2 does not bring much performance gain, indicating that a secondary DC bias of $\rho = 0.1$ is large enough to remove most of the zero samples in the time-domain signal and hence efficiently reduce the loss of spatial information. When the spectral efficiency is increased to 4 bits/s/Hz, the performance gap between FD/TD-GSM with $N = 2$ (i.e., RC) and FD/TD-GSMP with $N = 2$ (i.e., SMP) becomes only 1.5 dB. For a relatively high spectral efficiency of 5 bits/s/Hz, the best BER performance is obtained by FD/TD-GSMP with $N = 2$ (i.e., SMP) and an SNR gain of up to 6.5 dB can be achieved in comparison to FD/TD-GSM with $N = 2$ (i.e., RC). It can be seen from Fig. 7 that FD/TD-GSM with $N = 2$ (i.e., RC) performs better for a relatively low spectral efficiency due to its high diversity gain, while FD/TD-GSMP with $N = 2$ (i.e., SMP) achieves better performance for a relatively high spectral efficiency because of its high multiplexing gain.

Fig. 8 shows the BER versus transmitted SNR for OFDM-based 4×4 GO-MIMO at the receiver location of (1.5 m, 1.5 m, 0.85 m) with different spectral efficiencies. For OFDM-based FD-GSM/GSMP with a spectral efficiency of 3 bits/s/Hz, as shown in Fig. 8(a), the best BER performance is achieved by FD-GSM with $N = 4$ (i.e., RC) and the required SNR to reach BER $= 3.8 \times 10^{-3}$ is 136.4 dB. FD-GSM with $N = 4$ (i.e., RC) outperforms FD-GSMP with $N = 2$ by an SNR gain of 2.6 dB. For a spectral efficiency of 4 bits/s/Hz, as can be seen from Fig. 8(b), FD-GSMP with $N = 3$ performs the best and the BER performance of FD-GSMP with $N = 4$ (i.e., SMP) is slightly worse than FD-GSMP with $N = 3$. For a relatively high spectral efficiency of 5 bits/s/Hz, as shown in Fig. 8(c), the best BER performance is obtained by FD-GSMP with $N = 2$, which requires an SNR of 145.1 dB to reach BER $= 3.8 \times 10^{-3}$. Moreover, nearly the same BER performance can be achieved by FD-GSM with $N = 2$ and 3 in the small SNR region. It can be clearly observed from Figs. 8(a), (b) and (c) that error floors occur for FD-GSM with $N = 4$ (i.e., RC), when the spectral efficiency reaches 4 bits/s/Hz. For OFDM-based TD-GSM with a spectral efficiency of 3 bits/s/Hz, as shown in Fig. 8(d), the BER

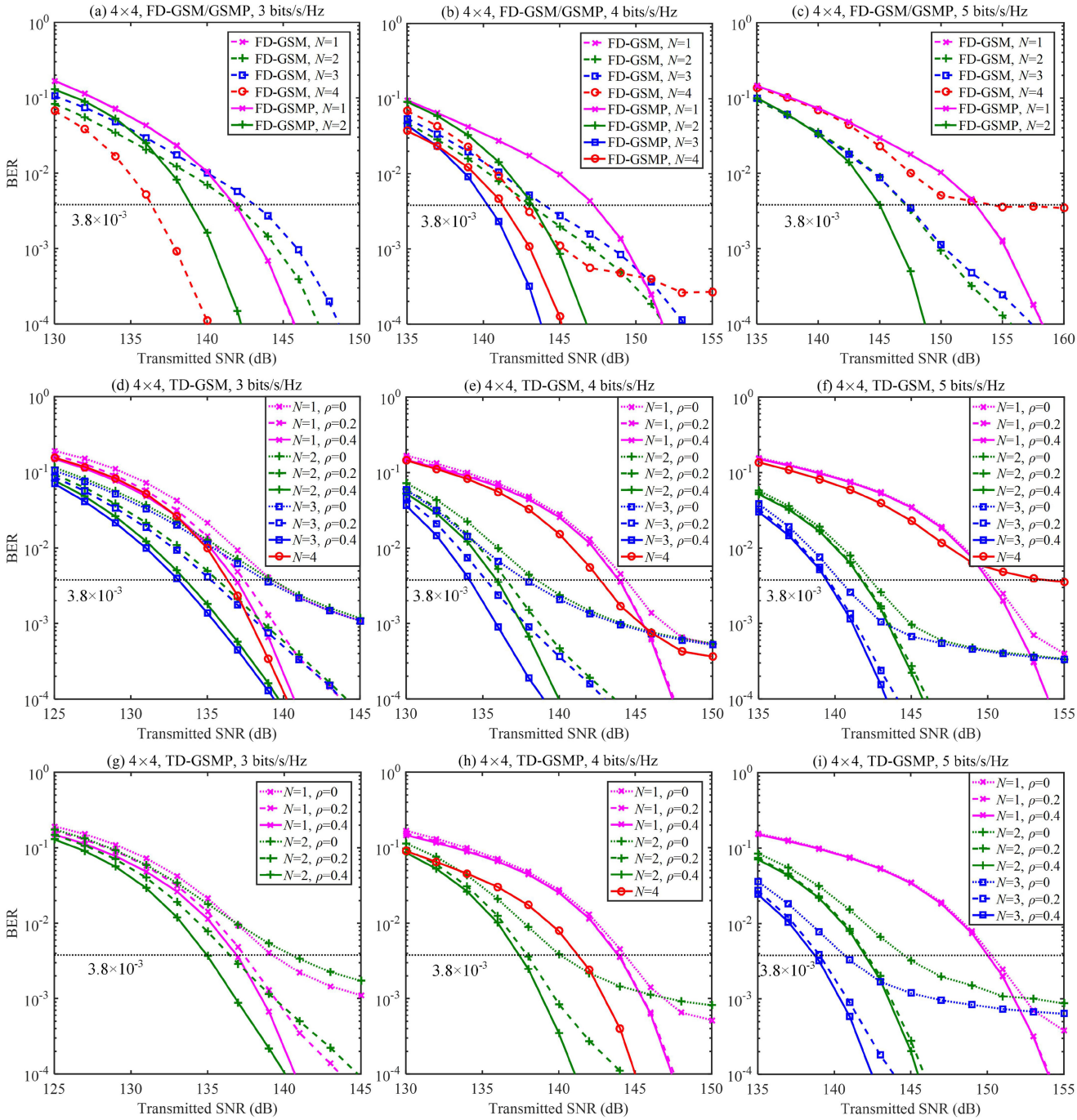

Fig. 8. BER vs. transmitted SNR for OFDM-based 4×4 GO-MIMO at the receiver location of (1.5 m, 1.5 m, 0.85 m) with (a) FD-GSM and FD-GSMP, 3 bits/s/Hz, (b) FD-GSM and FD-GSMP, 4 bits/s/Hz, (c) FD-GSM and FD-GSMP, 5 bits/s/Hz, (d) TD-GSM, 3 bits/s/Hz, (e) TD-GSM, 4 bits/s/Hz, (f) TD-GSM, 5 bits/s/Hz, (g) TD-GSMP, 3 bits/s/Hz, (h) TD-GSMP, 4 bits/s/Hz, and (i) TD-GSMP, 5 bits/s/Hz.

performance can be substantially improved when ρ is increased from 0 to 0.2 and further increasing ρ to 0.4 can only slightly improve the BER performance for all N values. For a higher spectral efficiency of 4 bits/s/Hz, as shown in Fig. 8(e), further increasing ρ to 0.4 does not bring improvement to TD-GSM with $N = 1$, indicating that a secondary DC bias with $\rho = 0.2$ is enough for TD-GSM with $N = 1$ to eliminate the loss of spatial information. In contrast, TD-GSM with $N = 2$ and 3 can still benefit from a higher secondary DC bias with $\rho = 0.4$. Specifically, SNR gains of 0.7 and 1.1 dB at BER $= 3.8 \times 10^{-3}$ can be further achieved by TD-GSM with $N = 2$ and 3, respectively, when ρ is increased from 0.2 to 0.4. For a spectral efficiency of 5 bits/s/Hz, as shown in Fig. 8(f), a secondary DC bias with $\rho = 0.2$ is enough for TD-GSM with all N values. It can be observed from Figs. 8(d), (e) and (f) that TD-GSM with $N = 3$ and $\rho = 0.4$ always achieves the best BER performance for the spectral efficiencies of 3, 4 and 5 bits/s/Hz. For OFDM-based TD-GSMP with a spectral efficiency of 3 bits/s/Hz and $\rho = 0$, as

TABLE VI
OPTIMAL GO-MIMO TECHNIQUES FOR VARIOUS SPECTRAL EFFICIENCIES UNDER 2×2 MIMO

Scenario	Optimal technique	Minimum SNR
3 bits/s/Hz	FD/TD-GSM, $N = 2$ (i.e., RC)	124.2 dB
4 bits/s/Hz	FD/TD-GSM, $N = 2$ (i.e., RC)	130.4 dB
5 bits/s/Hz	FD/TD-GSMP, $N = 2$ (i.e., SMP)	135.0 dB

TABLE VII
OPTIMAL GO-MIMO TECHNIQUES FOR VARIOUS SPECTRAL EFFICIENCIES UNDER 4×4 MIMO

Scenario	Optimal technique	Minimum SNR
3 bits/s/Hz	TD-GSM, $N = 3$, $\rho = 0.4$	133.1 dB
4 bits/s/Hz	TD-GSM, $N = 3$, $\rho = 0.4$	134.1 dB
5 bits/s/Hz	TD-GSMP, $N = 3$, $\rho = 0.4$	138.7 dB

shown in Fig. 8(g), TD-GSMP with $N = 2$ achieves better BER performance than that with $N = 1$ in the small SNR region, and TD-GSMP with $N = 1$ outperforms that with $N = 2$ when the SNR is larger than 136.8 dB. For both spectral efficiencies of 3 and 4 bits/s/Hz, TD-GSMP with $N = 2$ and $\rho = 0.4$ achieves the best BER performance. However, for a spectral efficiency of 5 bits/s/Hz, the best BER performance is obtained by TD-GSMP with $N = 3$ and $\rho = 0.4$.

According to Figs. 7 and 8, we can find that there exists an optimal GO-MIMO technique to achieve a target spectral efficiency given a specific receiver location. Table VI and Table VII summarize the optimal GO-MIMO techniques and the minimum required transmitted SNRs with spectral efficiencies of 3, 4 and 5 bits/s/Hz at the receiver location of (1.5 m, 1.5 m, 0.85 m) for 2×2 and 4×4 MIMO settings, respectively. For the 2×2 MIMO setting, FD/TD-GSM with $N = 2$ (i.e., RC) is found to be the optimal one for the relatively low spectral efficiencies of 3 and 4 bits/s/Hz, and the minimum required transmitted SNRs are 124.2 and 130.4 dB, respectively. For a relatively high spectral efficiency of 5 bits/s/Hz, FD/TD-GSMP with $N = 2$ (i.e., SMP) becomes the best one and the corresponding minimum required transmitted SNR is 135.0 dB. For the 4×4 MIMO setting, TD-GSM with $N = 3$ and $\rho = 0.4$ is the optimal one for the relatively low spectral efficiencies of 3 and 4 bits/s/Hz, while TD-GSMP with $N = 3$ and $\rho = 0.4$ is the best for a relatively high spectral efficiency of 5 bits/s/Hz.

Finally, we evaluate the BER performance of the proposed OFDM-based GO-MIMO techniques under the 4×4 MIMO setting by considering user mobility. Fig. 9 shows the BER versus receiver location across the receiving plane for OFDM-based 4×4 GO-MIMO with a spectral efficiency of 4 bits/s/Hz. For FD-GSM with a transmitted SNR of 146 dB, as shown in Fig. 9(a), an extremely high BER of about 0.4 is obtained by FD-GSM with $N = 1, 2$ and 3 when the receiver is located at the center of the room. It is mainly due to the geometric symmetry[5], which will lead to a less well conditioned channel matrix [40]. In contrast, FD-GSM with $N = 4$ (i.e., RC) can achieve a relatively stable BER performance over the central area of the room, which is mainly owing to its high spatial diversity. In addition, the BER performance of FD-GSM all N values is significantly degraded when the receiver is moving towards the corners, and the best BER performance across the room is achieved by FD-GSM with

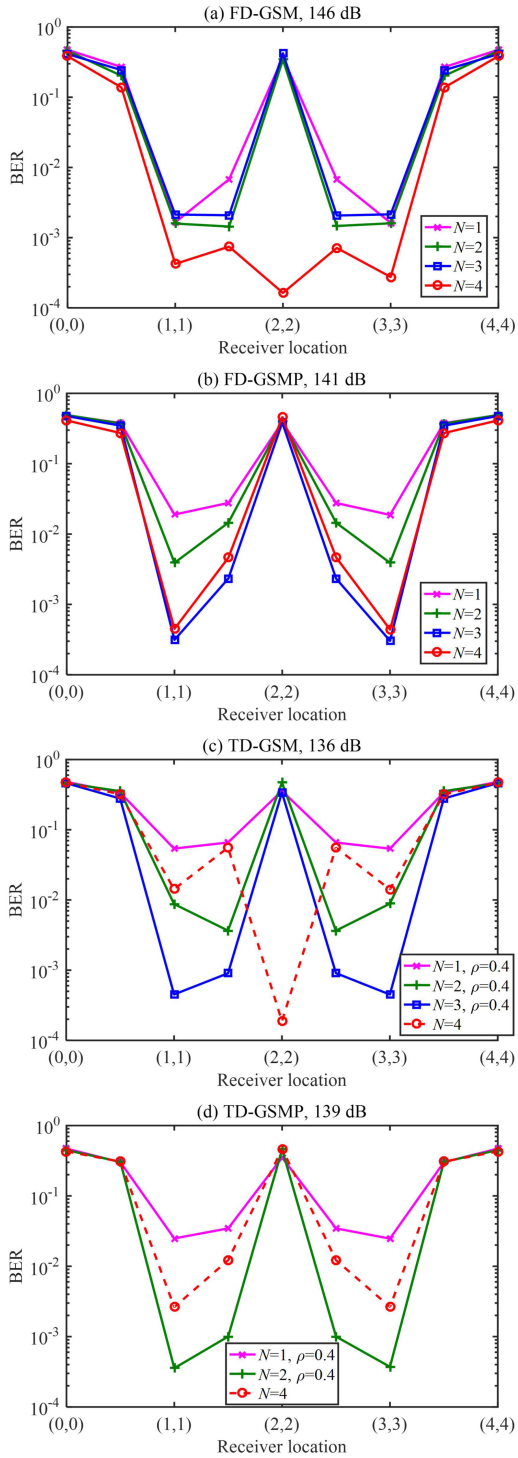

Fig. 9. BER vs. receiver location for OFDM-based 4×4 GO-MIMO with a spectral efficiency of 4 bits/s/Hz for (a) FD-GSM, (b) TD-GSM, (c) FD-GSMP and (d) TD-GSMP.

[5]The geometric symmetry-induced high channel correlation can be efficiently reduced by applying methods such as introducing power imbalance between the transmitters or blocking some of the links between the transmitters and receivers [5].

$N = 4$ (i.e., RC). For FD-GSMP with a transmitted SNR of 141 dB, as shown in Fig. 9(b), the BER fluctuates across the room for all N values, where the worst BER performance is achieved at the center and the corners of the room, while the best BER performance is obtained at the locations right under the LED transmitters. For TD-GSM with a transmitted SNR of 136 dB, as shown in Fig. 9(c), TD-GSM with $N = 1$, 2 and 3 performs the worst at the center due to geometric symmetry, while TD-GSM with $N = 4$ (i.e., RC) achieves the best BER performance at the center owing to its high spatial diversity. For TD-GSMP with a transmitted SNR of 139 dB, as shown in Fig. 9(d), the best BER performance across the room is achieved by TD-GSMP with $N = 2$ and $\rho = 0.4$. As can be seen from Fig. 9, the performance of OFDM-based GO-MIMO techniques is also highly related to the specific location of the receiver (i.e., user). Therefore, practical GO-MIMO systems can be designed in a user-centric manner, where an optimal GO-MIMO technique can be adaptively selected with respect to the specific location and spectral efficiency requirement of the user.

V. Conclusion

In this paper, we have proposed and evaluated four OFDM-based GO-MIMO techniques for bandlimited IM/DD OWC systems, including OFDM-based FD-GSM, FD-GSMP, TD-GSM and TD-GSMP. For OFDM-based FD-GSM and FD-GSMP, spatial mapping is performed in the frequency domain before OFDM modulation. In contrast, for OFDM-based TD-GSM and TD-GSMP, spatial mapping is conducted in the time domain after OFDM modulation. For each OFDM-based GO-MIMO technique, an ML detection algorithm is developed for efficient estimation of both spatial and constellation symbols. Particularly, for OFDM-based FD-GSM and TD-GSM, MRC is adopted for diversity combining after ML detection. To evaluate and compare the performance of the proposed OFDM-based GO-MIMO techniques, extensive simulations are performed in a typical indoor MIMO-OWC system under both 2×2 and 4×4 MIMO settings. Our results show that, for a given user location with a target spectral efficiency, there exists an optimal GO-MIMO technique to achieve the best BER performance. Moreover, the obtained optimal GO-MIMO technique might be different at different user locations. Therefore, a user-centric OFDM-based GO-MIMO system can be designed by adaptively selecting the optimal GO-MIMO technique according to the user's specific location and spectral efficiency requirement. In conclusion, the obtained results in this work might be able to shine some light on the design of a combined MIMO and OFDM scheme for bandlimited IM/DD OWC systems.

References

[1] T. Cogalan and H. Haas, "Why would 5G need optical wireless communications?" in *Proc. IEEE Ann. Int. Symp. Pers., Indoor Mobile Radio Commun.*, 2017, pp. 1–6.

[2] Z. Ghassemlooy, S. Arnon, M. Uysal, Z. Xu, and J. Cheng, "Emerging optical wireless communications-advances and challenges," *IEEE J. Sel. Areas Commun.*, vol. 33, no. 9, pp. 1738–1749, Sep. 2015.

[3] H. Elgala, R. Mesleh, and H. Haas, "Indoor optical wireless communication: Potential and state-of-the-art," *IEEE Commun. Mag.*, vol. 49, no. 9, pp. 56–62, Sep. 2011.

[4] S. Rajagopal, R. D. Roberts, and S.-K. Lim, "IEEE 802.15. 7 visible light communication: Modulation schemes and dimming support," *IEEE Commun. Mag.*, vol. 50, no. 3, pp. 72–82, Mar. 2012.

[5] T. Fath and H. Haas, "Performance comparison of MIMO techniques for optical wireless communications in indoor environments," *IEEE Trans. Commun.*, vol. 61, no. 2, pp. 733–742, Feb. 2013.

[6] C. Chen *et al.*, "User-centric MIMO techniques for indoor visible light communication systems," *IEEE Syst. J.*, vol. 14, no. 3, pp. 3202–3213, Sep. 2020.

[7] M. Z. Afgani, H. Haas, H. Elgala, and D. Knipp, "Visible light communication using OFDM," in *Proc. Int. Conf. Testbeds Res. Infrastructures Develop. Netw. Communities*, 2006, pp. 129–134.

[8] R. Mesleh, H. Elgala, and H. Haas, "On the performance of different OFDM based optical wireless communication systems," *J. Opt. Commun. Netw.*, vol. 3, no. 8, pp. 620–628, Aug. 2011.

[9] X. Zhang, S. Dimitrov, S. Sinanovic, and H. Haas, "Optimal power allocation in spatial modulation OFDM for visible light communications," in *Proc. IEEE Veh. Technol. Conf.*, 2012, pp. 1–5.

[10] Y. Li, D. Tsonev, and H. Haas, "Non-DC-biased OFDM with optical spatial modulation," in *Proc. IEEE Int. Symp. Pers., Indoor Mobile Radio Commun.*, 2013, pp. 486–490.

[11] I. Tavakkolnia, A. Yesilkaya, and H. Haas, "OFDM-based spatial modulation for optical wireless communications," in *Proc. IEEE Globecom Workshops*, 2018, pp. 1–6.

[12] A. Yesilkaya, R. Bian, I. Tavakkolnia, and H. Haas, "OFDM-based optical spatial modulation," *IEEE J. Sel. Topics Signal Process.*, vol. 13, no. 6, pp. 1433–1444, Oct. 2019.

[13] A. H. Azhar, T.-A. Tran, and D. O'Brien, "A gigabit/s indoor wireless transmission using MIMO-OFDM visible-light communications," *IEEE Photon. Technol. Lett.*, vol. 25, no. 2, pp. 171–174, Dec. 2012.

[14] T. Q. Wang, R. J. Green, and J. Armstrong, "MIMO optical wireless communications using ACO-OFDM and a prism-array receiver," *IEEE J. Sel. Areas Commun.*, vol. 33, no. 9, pp. 1959–1971, May 2015.

[15] Y. Hong, T. Wu, and L.-K. Chen, "On the performance of adaptive MIMO-OFDM indoor visible light communications," *IEEE Photon. Technol. Lett.*, vol. 28, no. 8, pp. 907–910, Jan. 2016.

[16] A. Yesilkaya, E. Basar, F. Miramirkhani, E. Panayirci, M. Uysal, and H. Haas, "Optical MIMO-OFDM with generalized LED index modulation," *IEEE Trans. Commun.*, vol. 65, no. 8, pp. 3429–3441, May 2017.

[17] A. Yesilkaya, T. Cogalan, E. Panayirci, H. Haas, and H. V. Poor, "Achieving minimum error in MISO optical spatial modulation," in *Proc. IEEE Int. Conf. Commun.*, 2018, pp. 1–6.

[18] A. Younis, N. Serafimovski, R. Mesleh, and H. Haas, "Generalised spatial modulation," in *Proc. Conf. Rec. Asilomar Conf. Signals, Syst., Comput.*, 2010, pp. 1498–1502.

[19] J. Fu, C. Hou, W. Xiang, L. Yan, and Y. Hou, "Generalised spatial modulation with multiple active transmit antennas," in *Proc. IEEE Globecom Workshops*, 2010, pp. 839–844.

[20] J. Wang, S. Jia, and J. Song, "Generalised spatial modulation system with multiple active transmit antennas and low complexity detection scheme," *IEEE Trans. Wireless Commun.*, vol. 11, no. 4, pp. 1605–1615, Apr. 2012.

[21] S. Alaka, T. L. Narasimhan, and A. Chockalingam, "Generalized spatial modulation in indoor wireless visible light communication," in *Proc. IEEE Glob. Commun. Conf.*, 2015, pp. 1–7.

[22] F. Wang, F. Yang, and J. Song, "Constellation optimization under the ergodic VLC channel based on generalized spatial modulation," *Opt. Exp.*, vol. 28, no. 14, pp. 21 202–21 209, Jul. 2020.

[23] K. Wang, "Indoor optical wireless communication system with filters-enhanced generalized spatial modulation and carrierless amplitude and phase (CAP) modulation," *Opt. Lett.*, vol. 45, no. 18, pp. 4980–4983, Sep. 2020.

[24] R. Mitra and V. Bhatia, "Chebyshev polynomial-based adaptive predistorter for nonlinear LED compensation in VLC," *IEEE Photon. Technol. Lett.*, vol. 28, no. 10, pp. 1053–1056, May 2016.

[25] H. Le Minh *et al.*, "100-Mb/s NRZ visible light communications using a postequalized white LED," *IEEE Photon. Technol. Lett.*, vol. 21, no. 15, pp. 1063–1065, Aug. 2009.

[26] C. Chen, W.-D. Zhong, and D. Wu, "Indoor OFDM visible light communications employing adaptive digital pre-frequency domain equalization," in *Proc. Conf. Lasers Electro-Opt.*, 2016, Paper JTh2A.118.

[27] A. A. Purwita, M. D. Soltani, M. Safari, and H. Haas, "Terminal orientation in OFDM-based LiFi systems," *IEEE Trans. Wireless Commun.*, vol. 18, no. 8, pp. 4003–4016, Aug. 2019.

[28] T. Komine and M. Nakagawa, "Fundamental analysis for visible-light communication system using LED lights," *IEEE Trans. Consum. Electron.*, vol. 50, no. 1, pp. 100–107, Feb. 2004.
[29] P. Chvojka, S. Zvanovec, P. Haigh, and Z. Ghassemlooy, "Channel characteristics of visible light communications within dynamic indoor environment," *J. Lightw. Technol.*, vol. 33, no. 9, pp. 1719–1725, Feb. 2015.
[30] A. Burton, H. Minh, Z. Ghassemlooy, E. Bentley, and C. Botella, "Experimental demonstration of 50-Mb/s visible light communications using $4\times$ 4 MIMO," *IEEE Photon. Technol. Lett.*, vol. 26, no. 9, pp. 945–948, May 2014.
[31] C. Chen, W.-D. Zhong, H. Yang, and P. Du, "On the performance of MIMO-NOMA-based visible light communication systems," *IEEE Photon. Technol. Lett.*, vol. 30, no. 4, pp. 307–310, Feb. 2018.
[32] D. Tsonev *et al.*, "A 3-Gb/s single-LED OFDM-based wireless VLC link using a gallium nitride μLED," *IEEE Photon. Technol. Lett.*, vol. 26, no. 7, pp. 637–640, Apr. 2014.
[33] S. D. Dissanayake and J. Armstrong, "Comparison of ACO-OFDM, DCO-OFDM and ADO-OFDM in IM/DD systems," *J. Lightw. Technol.*, vol. 31, no. 7, pp. 1063–1072, Apr. 2013.
[34] L. Yin, W. O. Popoola, X. Wu, and H. Haas, "Performance evaluation of non-orthogonal multiple access in visible light communication," *IEEE Trans. Commun.*, vol. 64, no. 12, pp. 5162–5175, Dec. 2016.
[35] C. Chen, W.-D. Zhong, H. Yang, S. Zhang, and P. Du, "Reduction of SINR fluctuation in indoor multi-cell VLC systems using optimized angle diversity receiver," *J. Lightw. Technol.*, vol. 36, no. 17, pp. 3603–3610, May 2018.
[36] E. Başar, Ü. Aygölü, E. Panayırcı, and H. V. Poor, "Orthogonal frequency division multiplexing with index modulation," *IEEE Trans. Signal Process.*, vol. 61, no. 22, pp. 5536–5549, Nov. 2013.
[37] E. Başar and E. Panayırcı, "Optical OFDM with index modulation for visible light communications," in *Proc. IEEE Int. Workshops Opt. Wireless Commun.*, 2015, pp. 11–15.
[38] C. Chen, W.-D. Zhong, H. Yang, P. Du, and Y. Yang, "Flexible-rate SIC-free NOMA for downlink VLC based on constellation partitioning coding," *IEEE Wireless Commun. Lett.*, vol. 8, no. 2, pp. 568–571, Apr. 2019.
[39] R. Bian, I. Tavakkolnia, and H. Haas, "15.73 gb/s visible light communication with off-the-shelf LEDs," *J. Lightw. Technol.*, vol. 37, no. 10, pp. 2418–2424, May 2019.
[40] L. Zeng *et al.*, "High data rate multiple input multiple output (MIMO) optical wireless communications using white LED lighting," *IEEE J. Sel. Areas Commun.*, vol. 27, no. 9, pp. 1654–1662, Dec. 2009.

Chen Chen (Member, IEEE) received the B.S. and M.Eng. degrees from the University of Electronic Science and Technology of China, Chengdu, China, in 2010 and 2013, respectively, and the Ph.D. degree from Nanyang Technological University, Singapore, in 2017. From 2017 to 2019, he was a Postdoctoral Researcher with the School of Electrical and Electronic Engineering, Nanyang Technological University. He is currently a Tenure-Track Assistant Professor with the School of Microelectronics and Communication Engineering, Chongqing University, Chongqing, China. His research interests include optical wireless communication, optical access networks, Internet of Things, and machine learning.

Xin Zhong is currently working toward the Ph.D. degree with the School of Microelectronics and Communication Engineering, Chongqing University, Chongqing, China. His research interests include optical wireless communication and MIMO transmission.

Shu Fu received the Ph.D. degree in communication and information system from the University of Electronic Science and Technology of China, Chengdu, China, in 2016, with a focus on cooperative multipoint (CoMP) wireless network, QoS routing in wavelength division multiplexing (WDM) network, and cross-network energy efficiency. He is currently an Associate Professor with the School of Microelectronics and Communication Engineering, Chongqing University, Chongqing, China. His research interests include the next generation of wireless networks, integrated networks, and network virtualization.

Xin Jian received the B.Eng. and Ph.D. degrees from Chongqing University, Chongqing, China, in 2009 and 2014, respectively. He is currently an Associate Professor with the School of Microelectronics and Communication Engineering, Chongqing University. His research interests include the Internet of Things, next-generation mobile communication, and wireless ad hoc networks.

Min Liu received the B.Eng. and M.Eng. degrees from Chongqing University, Chongqing, China, in 1997 and 2000, respectively, and the Ph.D. degree from Nanyang Technological University, Singapore, in 2004. She is currently a Professor and the Vice Dean of the School of Microelectronics and Communication Engineering, Chongqing University. Her main research interests include optical fiber communication and photonic crystal fibers.

Helin Yang (Member, IEEE) received the B.S. and M.S. degrees from the School of Telecommunications Information Engineering, Chongqing University of Posts and Telecommunications, Chongqing, China, in 2013 and 2016, respectively, and the Ph.D. degree from the School of Electrical and Electronic Engineering, Nanyang Technological University, Singapore, in 2020. His current research interests include wireless communication, visible light communication, the Internet of Things, and resource management.

Arokiaswami Alphones (Senior Member, IEEE) received the B.Tech. degree from the Madras Institute of Technology, Chennai, India, in 1982, the M.Tech. degree from the the Indian Institute of Technology Kharagpur, Kharagpur, India, in 1984, and the Ph.D. degree in optically controlled millimeter wave circuits from the Kyoto Institute of Technology, Kyoto, Japan, in 1992. Since 2001, he has been with the School of Electrical and Electronic Engineering, Nanyang Technological University, Singapore. His current research interests include electromagnetic analysis on planar RF circuits and integrated optics, microwave photonics, metamaterial-based leaky wave antennas, and wireless power transfer technologies.

H. Y. Fu (Senior Member, IEEE) received the B.S. degree in electronic and information engineering from Zhejiang University, Hangzhou, China, the M.S. degree in electrical engineering with specialty in photonics from the Royal Institute of Technology, Stockholm, Sweden, and the Ph.D. degree from the Department of Electrical Engineering, Hong Kong Polytechnic University, Hong Kong. He is currently an Associate Professor and Acting Co-Director of Data Science and Information Technology Research Center, Tsinghua-Berkeley Shenzhen Institute (TBSI), Tsinghua University, Beijing, China. From 2005 to 2010, he was a Research Assistant and then a Research Associate with Photonic Research Center, Hong Kong Polytechnic University. From 2010 to 2017, he was a Founding Member and leading the advanced fiber optic communications research with Central Research Institute, Huawei. His research interests include integrated photonics and its related applications, fiber optical communications, and fiber optical sensing technologies.